Article No. jmbi.1999.2841 available online at http://www.idealibrary.com on IDEAL® *J. Mol. Biol.* (1999) **289**, 1267–1282

JMB

Solution Structure and Thermodynamics of a Divalent Metal Ion Binding Site in an RNA Pseudoknot

Ruben L. Gonzalez Jr and Ignacio Tinoco Jr*

Department of Chemistry University of California Berkeley and Structural Biology Department, Physical Biosciences Division Lawrence Berkeley National Laboratory, Berkeley, CA 94720-1460 USA

**Corresponding author*

Identification and characterization of a metal ion binding site in an RNA pseudoknot was accomplished using cobalt (III) hexammine, $Co(NH_3)_6^{3+}$, as a probe for magnesium (II) hexahydrate, $Mg(H_2O)_6^{2+}$, in nuclear magnetic resonance (NMR) structural studies. The pseudoknot causes efficient −1 ribosomal frameshifting in mouse mammary tumor virus. Divalent metal ions, such as Mg^{2+}, are critical for RNA structure and function; Mg^{2+} preferentially stabilizes the pseudoknot relative to its constituent hairpins. The use of $Co(NH_3)_6^{3+}$ as a substitute for Mg^{2+} was investigated by ultraviolet absorbance melting curves, NMR titrations of the imino protons, and analysis of NMR spectra in the presence of Mg^{2+} or $Co(NH_3)_6^{3+}$. The structure of the pseudoknot-$Co(NH_3)_6^{3+}$ complex reveals an ion-binding pocket formed by a short, two-nucleotide loop and the major groove of a stem. $Co(NH_3)_6^{3+}$ stabilizes the sharp loop-to-stem turn and reduces the electrostatic repulsion of the phosphates in three proximal strands. Hydrogen bonds are identified between the $Co(NH_3)_6^{3+}$ protons and non-bridging phosphate oxygen atoms, 2′ hydroxyl groups, and nitrogen and oxygen acceptors on the bases. The binding site is significantly different from that previously characterized in the major groove surface of tandem G·U base-pairs, but is similar to those observed in crystal structures of a fragment of the 5 S rRNA and the P5c helix of the *Tetrahymena thermophila* group I intron. Changes in chemical shifts occurred at the same pseudoknot protons on addition of Mg^{2+} as on addition of $Co(NH_3)_6^{3+}$, indicating that both ions bind at the same site. Ion binding dissociation constants of approximately 0.6 mM and 5 mM (in 200 mM Na^+ and a temperature of 15 °C) were obtained for $Co(NH_3)_6^{3+}$ and Mg^{2+}, respectively, from the change in chemical shift as a function of metal ion concentration. An extensive array of non-sequence-specific hydrogen bond acceptors coupled with conserved structural elements within the binding pocket suggest a general mode of divalent metal ion stabilization of this type of frameshifter pseudoknot. These results provide new thermodynamic and structural insights into the role divalent metal ions play in stabilizing RNA tertiary structural motifs such as pseudoknots.

Keywords: RNA structure and thermodynamics; NMR; metal binding; pseudoknot; frameshifting

Introduction

The capacity of RNA to perform structural and functional roles in biological processes depends upon its ability to fold into complex and compact tertiary structures. The close packing of helices and loops that is required for the formation of these structures is opposed by the presence of the negatively charged phosphodiester backbone. Positive ions non-specifically stabilize RNA structure (Anderson & Record, 1995) by screening the nega-

Abbreviations used: MMTV, mouse mammary tumor virus; NOE, nuclear Overhauser effect; PK, pseudoknot; HP, hairpin; SS, single-strand; NOESY, NOE spectroscopy; HSQC, heteronuclear single quantum coherence; DQF-COSY, double quantum filtered correlated spectroscopy; ICP, inductively coupled plasma.

E-mail address of the corresponding author: itinoco@lbl.gov

0022-2836/99/251267–16 $30.00/0

tively charged backbone. Additionally, specific metal ion binding sites have been identified that are important in RNA structure and function (Stein & Crothers, 1976; Draper, 1985; Pan *et al.*, 1993; Laggerbauer *et al.*, 1994; Doudna & Doherty, 1997; Feig & Uhlenbeck, 1999). Until recently, detailed investigations of the interactions of metal ions with RNA was limited to crystallographic studies of tRNAs (Holbrook *et al.*, 1977; Jack *et al.*, 1977). Currently, crystal structures of hammerhead ribozymes (Scott *et al.*, 1995; Pley *et al.*, 1994), the P4-P6 domain of the *Tetrahymena thermophila* self-splicing group I intron (Cate *et al.*, 1996; Cate & Doudna, 1996), and a 5 S ribosomal RNA (rRNA) domain (Correll *et al.*, 1997) have revealed details of the interactions between divalent metal ions and specific binding sites in RNA. Some of these sites occur within elements of the secondary structure and others mediate tertiary contacts. The possibility of studying these types of interactions in solution using cobalt (III) hexammine ($Co(NH_3)_6^{3+}$) as an analog of fully hydrated magnesium (II) hexahydrate ($Mg(H_2O)_6^{2+}$) was suggested by Cowan (1993), based on similar ionic radii and covalent geometries for the two metal ion complexes, as well as evidence that $Co(NH_3)_6^{3+}$ can activate some Mg^{2+}-dependent enzymes (Jou & Cowan, 1991). Its use in solution nuclear magnetic resonance (NMR) structural studies has been demonstrated by Robinson & Wang (1995) in DNA decamers and by Kieft & Tinoco (1997) in the P5b stem-loop from the *T. thermophila* group I intron. These structural studies of $Co(NH_3)_6^{3+}$ binding to nucleic acid secondary structural elements prompted this study of the metal ion complex in the stabilization of RNA tertiary interactions in solution.

RNA pseudoknots are a classic family of tertiary structures formed when nucleotides in the loop of a hairpin pair with nucleotides from an adjacent single-stranded region, forming a second stem and loop (Pleij *et al.*, 1985). Pseudoknots have many different functional roles in biological systems. They occur at the 3′ termini of several plant virus RNA genomes (Haenni *et al.*, 1982; Rietveld *et al.*, 1982; Joshi, *et al.*, 1983; Guerrier-Takada *et al.*, 1988; Kolk *et al.*, 1998), in ribonuclease P RNA (James *et al.*, 1988), within 16 S rRNA (Moazed & Noller, 1987), and most recently a pseudoknot structure has been identified as a key component of a hepatitis delta virus ribozyme (Ferré-D'Amaré *et al.*, 1998). Pseudoknots are often involved in translational control (Tang & Draper, 1989; Schimmel, 1989), and cause programmed ribosomal frameshifting in many retroviruses (Chamorro *et al.*, 1992; ten Dam *et al.*, 1994, 1995; Brierley *et al.*, 1991; Chen *et al.*, 1995; Brierley, 1995). Several studies have investigated the thermodynamics of pseudoknot formation and stabilization (Wyatt *et al.*, 1990; Qui *et al.*, 1996; Theimer *et al.*, 1998; Nixon & Giedroc, 1998).

The VPK pseudoknot studied here (Shen & Tinoco, 1995) causes frameshifting in mouse mammary tumor virus (MMTV). It differs from the wild-type MMTV pseudoknot in that four of the G·C base-pairs were flipped to C·G base-pairs to disrupt G-rich tracks that led to multiple conformations in the native sequence (Figure 1(a) and (b)). The modified VPK sequence has equal frameshifting efficiency as the wild-type MMTV sequence in two different constructs of flanking sequences (Chen *et al.*, 1995). The VPK pseudoknot forms below 25 °C in the presence of 200 mM Na^+, but small concentrations of Mg^{2+} (10 μM) or $Co(NH_3)_6^{3+}$ (5 μM) greatly stabilize it. The higher charge of Mg^{2+} or $Co(NH_3)_6^{3+}$ compared to Na^+ undoubtedly contributes to the increased stability of the pseudoknot, but in addition there could be a specific metal ion binding site in the VPK pseudoknot. This specificity could be driven by the ionic radii and the octahedral coordination geometry of Mg^{2+} and $Co(NH_3)_6^{3+}$, compared to the smaller ionic radius and tetrahedral coordination geometry of Na^+.

Here, we present the solution structure and a thermodynamic study of a metal ion-RNA tertiary interaction: an RNA pseudoknot, stabilized by a specifically bound Co(III) ion complex. Nuclear Overhauser effect (NOE) crosspeaks between the protons of $Co(NH_3)_6^{3+}$ and 15 RNA protons allowed identification and characterization of the binding site. $Co(NH_3)_6^{3+}$ and Mg^{2+} stabilize the pseudoknot as shown by ultraviolet absorbance melting curves. NMR titration experiments demonstrated that $Co(NH_3)_6^{3+}$ and Mg^{2+} ions interact with the pseudoknot structure at the same site, and provided estimates of their binding constants. We expect similar electrostatic and hydrogen-bonding interactions of $Co(NH_3)_6^{3+}$ and $Mg(H_2O)_6^{2+}$ with the RNA, although the stability of binding is different.

Results

Thermodynamics

Ultraviolet absorbance melting curves

Ultraviolet (UV) absorbance melting curves for VPK RNA dialyzed into 10 mM sodium phosphate, 200 mM NaCl, 100 μM EDTA (pH 6.4) are shown in Figure 2. The UV melting curve in the absence of Mg^{2+} or $Co(NH_3)_6^{3+}$ (Figure 2(a)) displays two major melting transitions. The first transition has a melting temperature (t_m) of approximately 27 °C and is assigned to the melting of the pseudoknot interaction. The second transition has a t_m of approximately 63 °C and is attributed to the melting of the remaining hairpin. These transitions were assigned based on the UV melting curves of each of the individual hairpins (Figure 1(c) and (d)) which display one transition each with a t_m of approximately 83 °C and no transitions at lower temperatures. Overall, the pseudoknot melting transitions are unimolecular, as no increase in t_m is observed with increasing VPK concentration over a range of 3 to 300 μM. Analysis of the derivative absorbance

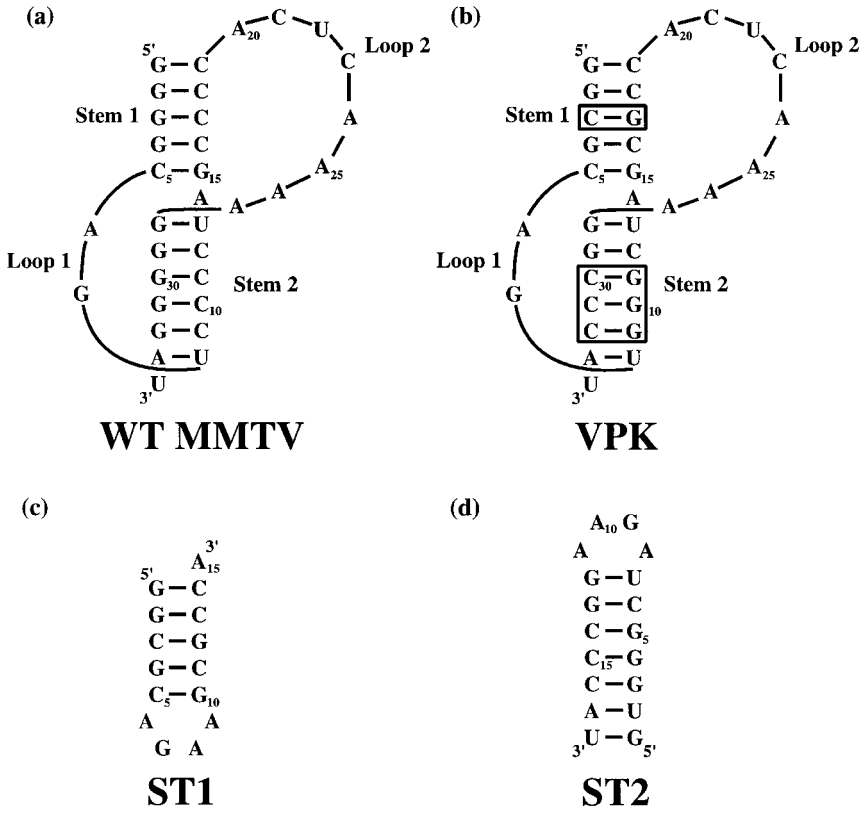

Figure 1. Sequence comparison of (a) wild-type MMTV pseudoknot and (b) the modified VPK pseudoknot. Boxed nucleotides indicate the changes made to facilitate NMR studies. The two pseudoknots have equal frameshifting efficiencies. (c) The ST1 hairpin was used as a model for stem 1 and (d) the ST2 hairpin was used as a model for stem 2 in UV absorbance melting experiments.

melting curve in the absence of multivalent ions yielded estimates of the standard enthalpy changes (ΔH^o) for the pseudoknot (PK) to hairpin (HP) transition and the hairpin (HP) to single-strand (SS) transition. As expected, due to the similarities of the two stems, the two ΔH^o values are within 10 % of each other ($\Delta H^o_{PK \rightarrow HP} \approx 37$ kcal mol^{-1} and $\Delta H^o_{HP \rightarrow SS} \approx 41$ kcal mol^{-1}). Titration of VPK RNA with $Co(NH_3)_6^{3+}$ (Figure 2(b)) or Mg^{2+} (Figure 2(c)) shifts the t_m of the two transitions to higher temperatures with increasing concentrations of metal ion until both transitions overlap. Completely overlapped transitions are observed at $Co(NH_3)_6^{3+}$ concentrations of 10 μM, or Mg^{2+} concentrations slightly higher than 50 μM. Shifts in t_m of approximately 40 deg. C for the first melting transition and 25 deg. C for the second melting transition are observed. Because the ΔH^o of the pseudoknot to hairpin transition is within 10 % of the ΔH^o of the hairpin to single-strand transition, the 15 deg. C difference between the two t_m shifts demonstrates that the multivalent ions preferentially bind to the pseudoknot relative to the hairpin or single-strand. Titrations with Na^+ (Figure 2(d)) also shift the t_m of the two transitions to higher temperatures with increasing concentrations of metal ion, albeit at much higher concentrations of Na^+. Even doubling the Na^+ concentration from 200 mM to 400 mM was not sufficient to produce overlapping transitions. The VPK pseudoknot requires approximately fivefold higher concentrations of Mg^{2+} than $Co(NH_3)_6^{3+}$ to achieve a similar degree of stabilization. Even with Na^+ concentrations at least 40,000-fold higher than $Co(NH_3)_6^{3+}$ concentrations, the same degree of pseudoknot stabilization is not attained. In the case of Na^+, t_m shifts of 30 deg. C and 25 deg. C are observed for the first and second melting transitions, respectively. The pseudoknot interaction is somewhat preferentially stabilized over the hairpin interaction, with only a 5 deg. C difference between the two shifts. These results are consistent with previous findings that very high concentrations of Na^+ are necessary in order for Na^+ to replace the stabilizing role of divalent ions in pseudoknots (Wyatt *et al.*, 1990).

Equilibrium binding constants

Imino proton resonance assignments were based on those made previously for VPK RNA in 5 mM $MgCl_2$ (Shen & Tinoco, 1995). VPK RNA was titrated with either $Co(NH_3)_6^{3+}$ or Mg^{2+} and the chemical shifts of the imino proton resonances were monitored as a function of concentration (Figure 3(a) and (b)). Chemical shift changes due to $Co(NH_3)_6^{3+}$ binding are very similar to those induced by Mg^{2+} binding. This indicates similar binding modes for both metal ions. In both cases the imino protons of G15, G17, and G4 exhibit the largest downfield shifts, whereas the imino protons of G9 and G11 undergo the largest upfield shifts. The imino protons of G1 and G2 are shifted to a greater degree by Mg^{2+}. This is presumably due to direct coordination of Mg^{2+} ions to the 5′-terminal

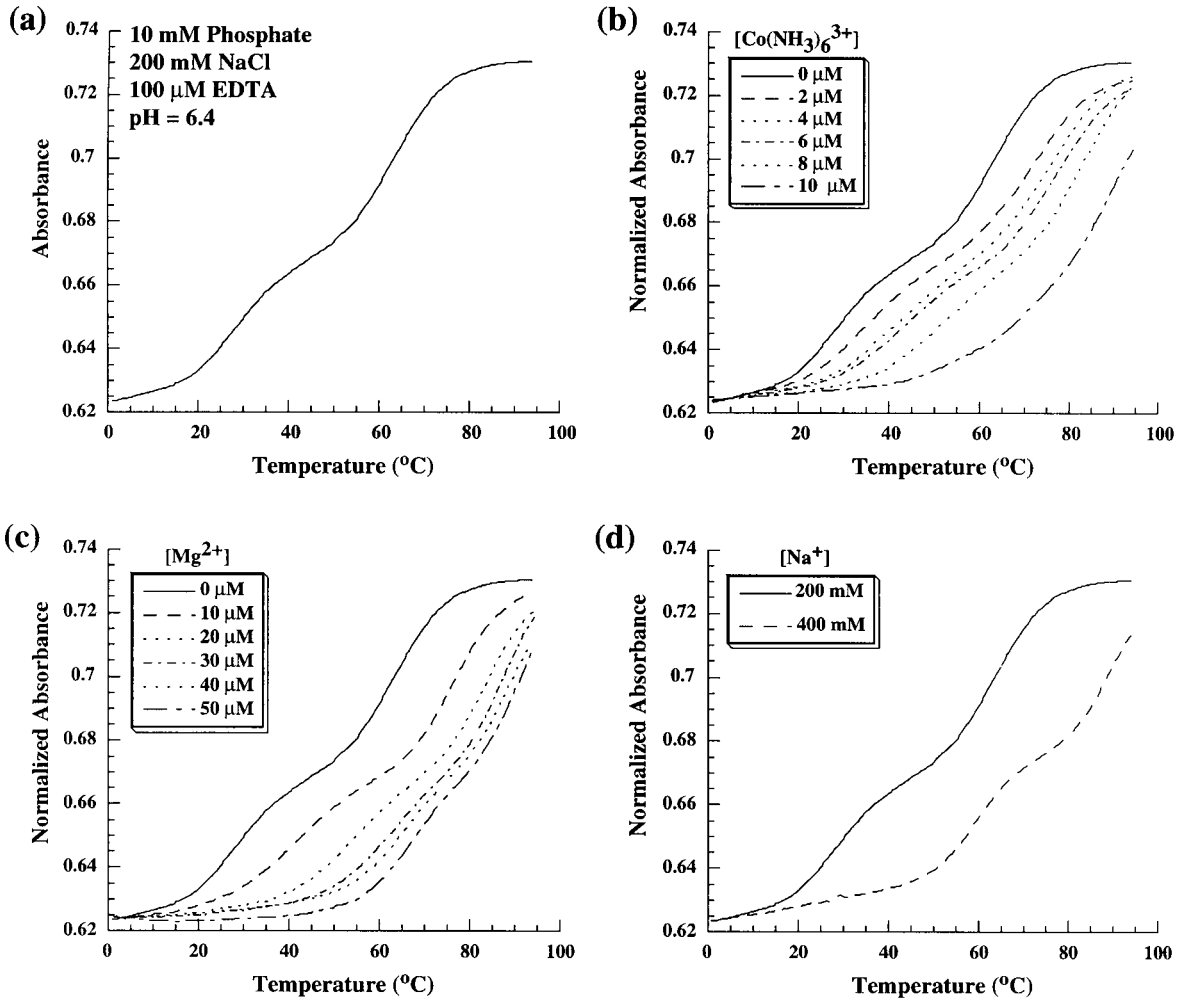

Figure 2. UV melting curves of the VPK pseudoknot. The VPK concentration in all melts is 4 μM. All samples were dialyzed against a buffer solution of 10 mM sodium phosphate, 200 mM NaCl, 100 μM EDTA (pH 6.4). Melting curves were acquired in the presence of (a) no additional salt, (b) 0-10 μM $Co(NH_3)_6^{3+}$, (c) 0-50 μM Mg^{2+}, and (d) 200 and 400 mM Na^+. The absorbances in (b), (c), and (d) are normalized with respect to the absorbance of (a).

triphosphate which does not occur with $Co(NH_3)_6^{3+}$ ions. Proton chemical shift changes can be caused by metal ion binding in the local environment of the proton, or by structural changes brought about by metal ion binding not necessarily near the proton. A H_2O NOE spectroscopy (NOESY) experiment in the presence of $Co(NH_3)_6^{3+}$ identified the imino protons which are directly near the binding site. NOE crosspeaks from $Co(NH_3)_6^{3+}$ protons to the imino protons of G10, G11, and G29 were observed, identifying these imino protons as direct probes of the metal ion binding site (Figure 4).

Binding curves can be constructed by plotting the chemical shift of individual imino protons as a function of metal ion concentration. Two such curves are plotted in Figure 3(b) for the imino proton of G11 *versus* $Co(NH_3)_6^{3+}$ and Mg^{2+} concentrations, respectively. For a system in fast exchange, the binding data for a 1:1 stoichiometry can be fit to the following binding isotherm:

$$\delta_{obs} = \delta_f + (\delta_b - \delta_f \times \left[\frac{([ion]_t + [RNA]_t + K_d) - \sqrt{([ion]_t + [RNA]_t + K_d)^2 - 4[RNA]_t \cdot [ion]_t}}{2[RNA]_t} \right]$$

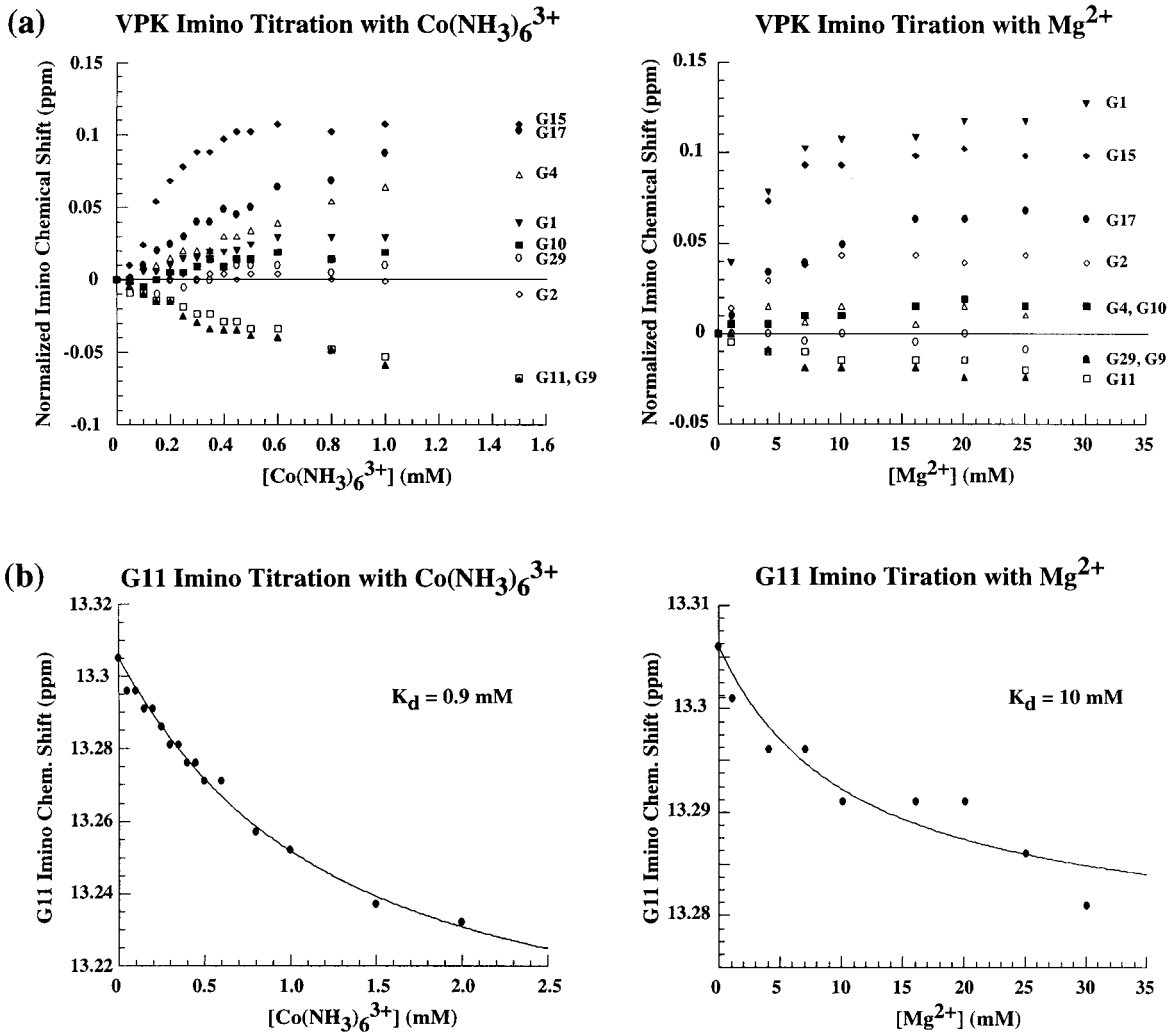

Figure 3. Imino proton titrations of VPK with $Co(NH_3)_6^{3+}$ and Mg^{2+}. The sample conditions are 400 μM VPK, 10 mM sodium phosphate, 200 mM NaCl, 100 μM EDTA (pH 6.4) at a temperature of 15 °C. (a) Plot of chemical shift *versus* $Co(NH_3)_6^{3+}$ and Mg^{2+} for all observed imino protons. The pattern of chemical shift changes are very similar for both metal ion complexes. (b) Binding curves for the G11 imino binding to $Co(NH_3)_6^{3+}$ and Mg^{2+}. Equilibrium dissociation constants (K_d) are calculated by fitting the data to a one binding site model.

in which δ_{obs} is the observed RNA chemical shift, δ_b is the chemical shift of the fully bound proton, δ_f is the chemical shift of the unbound proton, $[RNA]_t$ is the total RNA concentration, $[ion]_t$ is the total ion concentration, and K_d is the equilibrium binding dissociation constant for the RNA-metal ion complex (Roberts, 1993). This binding isotherm applies to one ion binding site per RNA molecule; it can be fit to obtain the fully bound chemical shift and the equilibrium binding dissociation constant K_d. Binding constants calculated for imino protons with significant chemical shift dependence on metal ion concentration agree within three- to fourfold of those calculated for the imino proton of G11 (Figure 3(b)), consistent with a one binding site model. This method was used to obtain equilibrium dissociation constants of $K_d(Co(NH_3)_6^{3+}) = 0.6(\pm 0.4)$ mM and $K_d(Mg^{2+}) = 5(\pm 3)$ mM, for binding to VPK in 10 mM sodium phosphate, 200 mM Na^+, 100 μM EDTA (pH 6.4), at a temperature of 15 °C. There is an approximately eightfold increase in affinity for the $Co(NH_3)_6^{3+}$ metal ion *versus* Mg^{2+} metal ion, presumably due to the greater positive charge of $Co(NH_3)_6^{3+}$. Although it would be advantageous to measure binding constants using a VPK non-exchangeable proton, no non-exchangeable proton resonance was sufficiently well resolved in the 1D spectra.

In addition to the imino protons at the Co $(NH_3)_6^{3+}$ binding site, imino protons from other regions of the pseudoknot display chemical shift changes. Imino protons from G17 and G4 in stem 1 exhibit downfield chemical shifts on binding of the cobalt ion complex. The G15 imino proton, adjacent to the junction region of the pseudoknot, demonstrates the largest chemical shift change in both the $Co(NH_3)_6^{3+}$ and Mg^{2+} titrations. It is clear that during these titrations considerable structural changes are occurring within the pseudoknot, particularly the junction region, which cause these

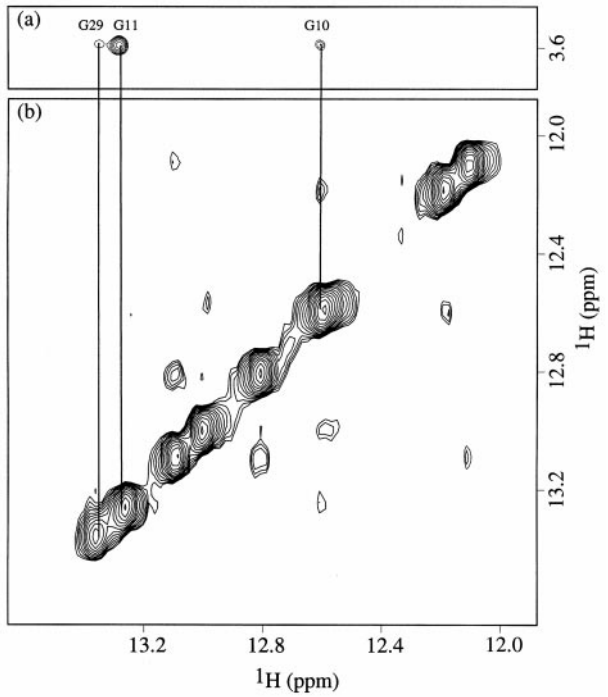

Figure 4. (a) Imino to $Co(NH_3)_6^{3+}$ and (b) imino to imino region of the 300 ms mixing time H_2O NOESY of the VPK pseudoknot in the presence of $Co(NH_3)_6^{3+}$. Lines show connectivities for the intermolecular NOE crosspeaks of the $Co(NH_3)_6^{3+}$ ammine protons with the imino proton diagonal peaks. Sample conditions are 2 mM VPK, 2 mM $Co(NH_3)_6^{3+}$, 10 MM sodium phosphate, 200 mM NaCl, 100 μM EDTA (pH 6.4), at a temperature of 20 °C.

chemical shift changes. Thus, unlike the P5b stem loop (Kieft & Tinoco, 1997), the pseudoknot structure changes upon divalent metal ion binding. Even small changes in the relative position of the G15 imino with respect to A6, A14, and/or A27 nucleotides at the junction may cause notable chemical shift changes due to the large ring currents associated with the adenine bases. Spectra acquired in 200 mM Na^+ but in the absence of Mg^{2+} or $Co(NH_3)_6^{3+}$ exhibit very broad, low intensity or absent NOE crosspeaks in the junction region. This may be due to low pseudoknot stability in the absence of Mg^{2+} or $Co(NH_3)_6^{3+}$ at higher temperatures, and/or broadening due to large rotational correlation times associated with lower temperatures. These broad or absent NOE crosspeaks, coupled with significant spectral overlap in the one dimensional spectra made it difficult to measure chemical shift changes for non-exchangeable protons in the junction region.

Similar binding studies were done and equilibrium binding dissociation constants were obtained for the $Co(NH_3)_6^{3+}$ binding site formed by tandem G·U base-pairs in the P5b stem loop from the *T. thermophila* group I intron (Kieft & Tinoco, 1997). The dissociation constant determined from imino proton titrations in 10 mM sodium phosphate, 200 mM Na^+, 100 μM EDTA (pH 6.4), and a temperature of 10 °C was $K_d = 0.19(\pm 0.01)$ mM (Kieft, 1997). Subsequent equilibrium dialysis experiments were done on P5b to validate the binding constants using imino proton chemical shift changes observed during metal ion titrations. The results of the equilibrium dialysis experiments are consistent with one metal ion binding at one strong binding site ($K_d = 0.72(\pm 0.06)$ mM) and approximately two ions binding at weaker binding sites ($K_d = 0.06(\pm 0.04)$ mM^2). The equilibrium dialysis K_d of the one strong binding site is about fourfold weaker binding than that calculated from the imino titrations. The K_d obtained from the imino proton titrations is expected to be smaller (stronger binding) than the value obtained from equilibrium dialysis due to assumptions about non-specific binding used in the analysis of the imino proton titration data. Non-specific binding leads to a decrease in the concentration of free $Co(NH_3)_6^{3+}$; in the equilibrium dialysis experiments, the free concentration of $Co(NH_3)_6^{3+}$ is determined directly, and the effect of non-specific binding is included. Nevertheless, using imino proton chemical shift changes during metal ion titrations provides equilibrium binding constants for strong binding sites that are in reasonable agreement with those measured from equilibrium dialysis experiments.

Comparison of spectra in Mg^{2+} and in $Co(NH_3)_6^{3+}$

NOESY spectra were acquired in H_2O and ^2H_2O for VPK in the presence of Mg^{2+} and in the presence of $Co(NH_3)_6^{3+}$. In both cases the same NOE connectivities and relative intensities are observed. The most notable changes occur in the chemical shifts of the RNA protons. It was observed that for VPK in the presence of Mg^{2+} the optimum temperature for experiments involving exchangeable protons was 15 °C, and for experiments involving non-exchangeable protons it was 30 °C. At these temperatures the VPK-$Co(NH_3)_6^{3+}$ complex displayed very broad lines and a number of NOE crosspeaks were not observed due to the line broadening. The VPK-$Co(NH_3)_6^{3+}$ complex displayed optimal spectral qualities at temperatures of 20 °C for exchangeable protons, and 35 °C for non-exchangeable protons. This is probably due to greater stabilization of VPK by 2 mM $Co(NH_3)_6^{3+}$ as compared to 5 mM Mg^{2+}. As indicated by the UV absorbance melting curves, about fivefold higher concentrations of Mg^{2+} are necessary to provide the same amount of stabilization as 2 mM $Co(NH_3)_6^{3+}$. Unfortunately, such large concentrations of Mg^{2+} generally tend to broaden spectral lines. The greater stabilization by $Co(NH_3)_6^{3+}$ allows for work at higher temperatures and provides sharper lines. Aggregation due to Mg^{2+} ions interacting with 5′ triphosphate groups on multiple VPK molecules may also cause broader lines in the Mg^{2+} spectra. This type of aggregation would not be present in the $Co(NH_3)_6^{3+}$ spectra.

Analysis of exchangeable proton resonances

Spectra recorded in H_2O displayed the same number of imino proton resonances for VPK in the presence of Mg^{2+} as in the presence of $Co(NH_3)_6^{3+}$. The same imino to imino NOE crosspeaks were observed in both complexes. There were no changes in the base-pairing scheme upon addition of $Co(NH_3)_6^{3+}$ as has been observed in the NMR structure of a fragment of 16 S rRNA that binds to ribosomal protein S8 (Kalurachchi & Nikonowicz, 1998). In addition, the same imino to amino, imino to H5 and imino to H1′ NOE crosspeak connectivities were observed for VPK in the presence of either Mg^{2+} or $Co(NH_3)_6^{3+}$. Assignments for exchangeable protons in the presence of Mg^{2+} at 15 °C and $Co(NH_3)_6^{3+}$ at 20 °C are provided in the Supplementary Material.

Analysis of non-exchangeable proton resonances

The sugar H1′ to base aromatic H6/H8 NOE crosspeak connectivities that are typical of *A*-form helical structure can be followed through both stems of the pseudoknot in the presence of either metal ion complex. The relative intensities of these crosspeaks are the same in both cases. In some regions of the spectra, better dispersion is obtained in the presence of $Co(NH_3)_6^{3+}$. In addition, connectivities observed through the pseudoknot loops in the presence of Mg^{2+} are also seen in the presence of $Co(NH_3)_6^{3+}$ (Figure 5(a) and (b)). As noted above, significant structural changes do occur upon metal binding in VPK, particularly in the junction region. The comparison of spectra in Mg^{2+} and in $Co(NH_3)_6^{3+}$ demonstrates that these changes occur in the presence of either metal ion complex, and that there is not much structural difference between the structure in the presence of Mg^{2+} or the presence of $Co(NH_3)_6^{3+}$. Assignments for non-exchangeable protons in the presence of Mg^{2+} at 30 °C and $Co(NH_3)_6^{3+}$ at 35 °C are provided in the Supplementary Material.

Intermolecular NOE crosspeak assignment

NOESY experiments in H_2O were used to detect intermolecular NOE crosspeaks between the Co

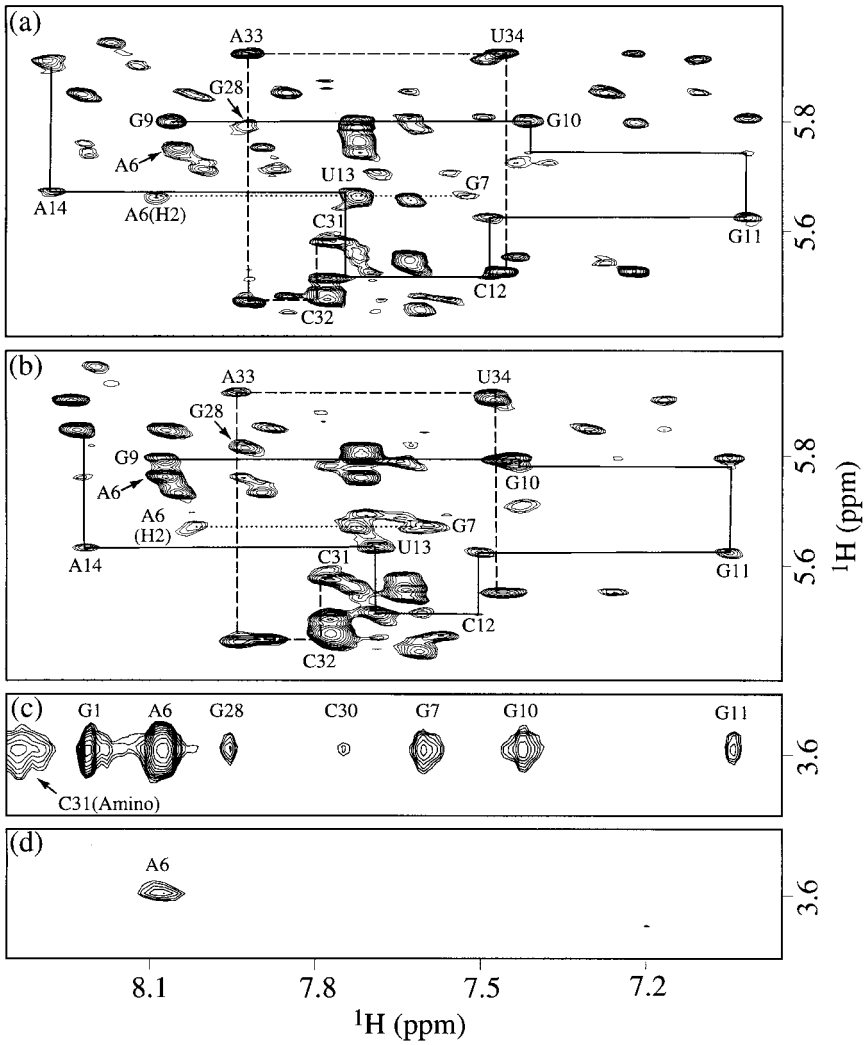

Figure 5. Aromatic to H1′ region of a 400 ms ^2H_2O NOESY of the VPK pseudoknot in the presence of (a) 5 mM Mg^{2+} and (b) 2 mM $Co(NH_3)_6^{3+}$. The continuous and broken lines indicate standard *A*-form walks for the two strands of stem 2. The dotted line indicates the A6H2 to G7H8 connectivity that is observed in loop 1. Arrows denote the A6 and the G28 intranucleotide H8 to H1′ NOE. (c) The $Co(NH_3)_6^{3+}$ proton to H6/H8 region of a 300 ms H_2O NOESY experiment. Intermolecular NOE crosspeaks are observed between $Co(NH_3)_6^{3+}$ protons and the H6/H8 proton of the denoted nucleotide. (d) The $Co(NH_3)_6^{3+}$ proton to H6/H8 region of a ^{13}C-resolved HSQC-NOESY on a VPK sample selectively ^{13}C-labeled at the adenine C8 and the uracil C6. Only one crosspeak, to the A6H8, is observed. Sample conditions in (a) are 2 mM VPK, 5 mM Mg^{2+}, 10 mM sodium phosphate, 200 mM NaCl, 100 μM EDTA (pH 6.4) at a temperature of 30 °C. Sample conditions in (b), (c) and (d) are identical, with the exception of 2 mM $Co(NH_3)_6^{3+}$ instead of 5 mM Mg^{2+}, and a temperature of 35 °C.

$(NH_3)_6^{3+}$ protons and the RNA protons. A total of 15 positive crosspeaks (same sign as diagonal peaks) were detected with varying intensities and line widths. Crosspeaks from the $Co(NH_3)_6^{3+}$ protons to the G10, G11, and G29 imino (Figure 4) and C12, C30, and C31 amino (Figure 5(c)) protons were assigned from the H_2O NOESY data.

Intermolecular NOE crosspeaks to aromatic RNA protons were more difficult to assign due to resonance overlap. The H_2O NOESY experiments at different concentrations of $Co(NH_3)_6^{3+}$ were used to determine which crosspeaks appeared first and with what intensity. Titration with $Co(NH_3)_6^{3+}$ gave rise to a set of peaks whose intensities increased with increasing concentrations of $Co(NH_3)_6^{3+}$; these peaks were assigned to a strong ion binding site. At higher concentrations of ligand, crosspeaks due to non-specific $Co(NH_3)_6^{3+}$ binding began to be observed. These results are consistent with one relatively strong binding site.

The ^2H_2O NOESY experiments at 20 °C and 35 °C provided chemical shift assignments for aromatic RNA protons at the two different temperatures. These were then compared with H_2O NOESY experiments recorded at the same temperatures. From these experiments it was possible to provide assignments for all but one of the intermolecular NOE crosspeaks. NOE crosspeaks were detected between the $Co(NH_3)_6^{3+}$ protons and the G1H8, G7H8, G10H8, G11H8, G28H8 and C30H6 (Figure 5(c)). The G1H8 is attributed to binding at the 5′-terminal triphosphate; addition of small amounts of Mg^{2+} to the $Co(NH_3)_6^{3+}$-VPK complex diminished the intensity of this crosspeak significantly without altering the intensity of the other peaks. The unassigned peak was the strongest intermolecular NOE crosspeak observed and, due to overlap of the A6H8 and the G9H8 resonances, could not be unambiguously assigned from the H_2O NOESY data of the unlabeled pseudoknot. This intermolecular crosspeak was unambiguously assigned as the A6H8 using an RNA sample specifically ^{13}C-labeled at the adenine C8 and uracil C6 position. An HSQC-NOESY experiment done in 90 % H_2O/10 % ^2H_2O was used to detect NOE crosspeaks from adenine H8 and uracil H6 protons. In the intermolecular $Co(NH_3)_6^{3+}$ proton to RNA aromatic proton region of this spectrum, only one crosspeak was observed and that was to the A6H8 (Figure 5(d)). The fact that no intermolecular crosspeaks to adenosine nucleotides at or near the junction are observed is consistent with no $Co(NH_3)_6^{3+}$ binding in this region of the pseudoknot. Also, no intermolecular crosspeaks are observed to any of the five adenine H8 s in loop 2 of the pseudoknot, again consistent with no $Co(NH_3)_6^{3+}$ binding in this region of the pseudoknot.

Structure calculations

A total of 100 starting structures were generated with randomized backbone torsion angles and randomized position of $Co(NH_3)_6^{3+}$. These initial structures were then subjected to the global fold protocol as described in Materials and Methods. Of the 100 starting structures, 30 structures converged with low NOE energies and total energies. These converged structures were then subjected to further refinement and energy minimization (see Materials and Methods). After refinement and energy minimization, 26 of the 30 structures were judged as acceptable structures based on low NOE energies and total energies, as well as lack of NOE violations greater than 0.2 Å. These 26 structures were used to determine the structure statistics shown in Table 1.

Discussion

VPK pseudoknot structure

The structure of the VPK pseudoknot in the presence of $Co(NH_3)_6^{3+}$ does not vary significantly from the structure determined in Mg^{2+} (Shen & Tinoco, 1995), although there are slight differences. Due to a number of new intramolecular RNA NOE crosspeaks, the intermolecular $Co(NH_3)_6^{3+}$ proton to RNA proton NOE crosspeaks, and a larger initial set of starting structures, the structure of the pseudoknot is now better defined. Stem 1 and stem 2 are fairly well defined in the 26 converged structures, with RMS deviations from the average structure of 0.81 Å and 1.09 Å, respectively. Intermolecular NOE crosspeaks from $Co(NH_3)_6^{3+}$ protons to RNA protons have bridged the gap between the short, two-nucleotide loop 1 and the major groove of stem 2, providing indirect loop-to-stem constraints; information that was previously unavailable. This has allowed better definition of loop 1, although the A6 and G7 bases in loop 1 can point out into solution or in towards stem 2, and

Table 1. Summary of NMR data and structural constraints

Constraints	
Intraresidue NOEs	69
Interresidue NOEs	117
Intermolecular NOEs	15
Hydrogen bonding	45
Torsion angle	279
Convergence	26/100
Violations	
NOE >0.2 Å	0
Torsion angle >10°	0
RMS deviations from ideal covalent geometry	
Bond lengths (Å)	0.004
Bond angles (deg.)	0.83
Impropers (deg.)	0.23
RMS deviations for converged structures	
All atoms (Å)	3.62 (2.41 for family 1, 2.81 for family 2)[a]
All atoms except loop 2 (Å)[b]	2.42
Binding site (Å)[c]	2.01

[a] Families were defined based on the two general geometries adopted by loop 2 as it enters the junction region. See Figure 6. There are 14 structures in family 1 and 12 in family 2.
[b] Residues 1-19, 28-34.
[c] Residues 6-13, 28-34.

still satisfy the NOE data available. The larger loop 2 is much more difficult to place with respect to stem 1. One critical, previously unassigned, NOE crosspeak was detected between the A27 H1′ in loop 2 and the G17 H1′ in stem 1. This crosspeak is observed in the presence of Mg^{2+} or $Co(NH_3)_6^{3+}$. Although it is clear that loop 2 crosses the minor groove of stem 1, it is not clear exactly how it does so. As can be seen in Figure 6 and Table 1, the two stems and loop 1 of the VPK pseudoknot superimpose relatively well, with an RMSD to the average structure of 2.42 Å. Loop 2, however, is not well defined and seems to adopt a number of possible conformations. Although this is mainly due to the lack of NOE and torsion angle constraints, there is evidence to support a dynamic loop 2. In DQF-COSY experiments, H5-H6 crosspeaks for loop residues C21, U22, and C23 are of higher intensity than H5-H6 crosspeaks for residues in the stem regions. Because the H5-H6 scalar coupling is constant, the observed difference in intensities indicate fast internal dynamics relative to the stem regions. Although this does not rule out the existence of alternate relaxation pathways, which may lead to broadening of the stem H5-H6 crosspeaks and thus lower intensity peaks, additional NMR evidence support a dynamic loop 2. The adenine H2 resonances are usually the sharpest peaks in the NMR spectra of RNA due to favorable relaxation properties, yet the H2 resonances of A26 and A27 in loop 2 are not detected. Furthermore, the structures were analyzed in order to identify protons within 3 Å and within 5 Å of loop 2 nucleotide protons. For each structure, roughly ten unique NOE crosspeaks are predicted involving loop 2 to stem 1 or loop 2 to loop 2 nucleotides that are not observed. The absence of these NOE crosspeaks could be caused by rapid internal motion of loop 2, leading to smaller local correlation times for these protons. Taken together, these data are consistent with a dynamic loop 2.

$Co(NH_3)_6^{3+}$ binding site

The $Co(NH_3)_6^{3+}$ ion binds in a pocket consisting of loop 1 and stem 2 residues (Figure 7). The short, two-nucleotide loop 1 must cross the major groove of the six base-pair stem 2, causing a sharp loop-to-stem turn and bringing the loop into close contact with the stem. This close contact is particularly unfavorable because of the repulsion of negatively charged phosphates on the three strands. The $Co(NH_3)_6^{3+}$ ion shields the electrostatic repulsion, and mediates this close interaction between the loop 1 and stem 2 by forming hydrogen bonds to the nitrogen and oxygen acceptors that are available on the surface of this binding pocket.

The $Co(NH_3)_6^{3+}$ ion is in the fast exchange regime within the binding pocket as well as in fast exchange between the bound and free forms as evidenced by a single average resonance frequency for all 18 $Co(NH_3)_6^{3+}$ protons. The structure calcu-

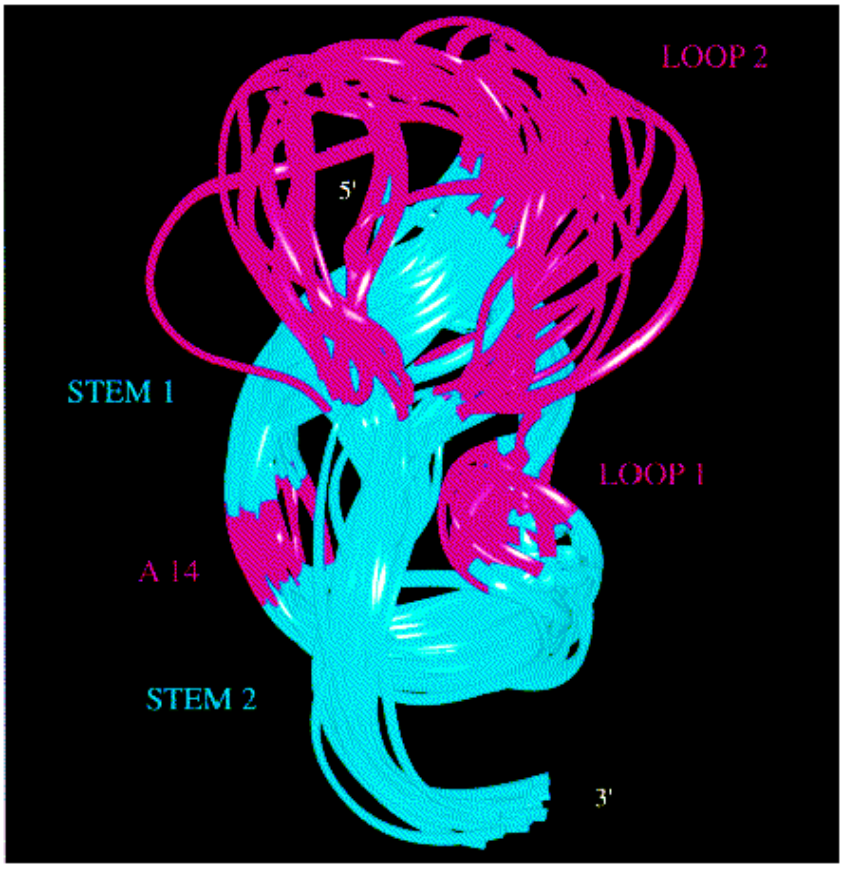

Figure 6. Superposition of the 26 converged VPK structures on the basis of all atoms for all residues excepting loop 2 residues. Loop 2 is observed to adopt a number of possible conformations as it crosses the minor groove of stem 1. There are, however, two general geometries adopted by loop 2 as it enters the junction region, allowing for the definition of two general families of structures. Loops and the junction A14 nucleotide are shown in magenta and stems in cyan. The RMS deviation from the average structure is 2.42 Å.

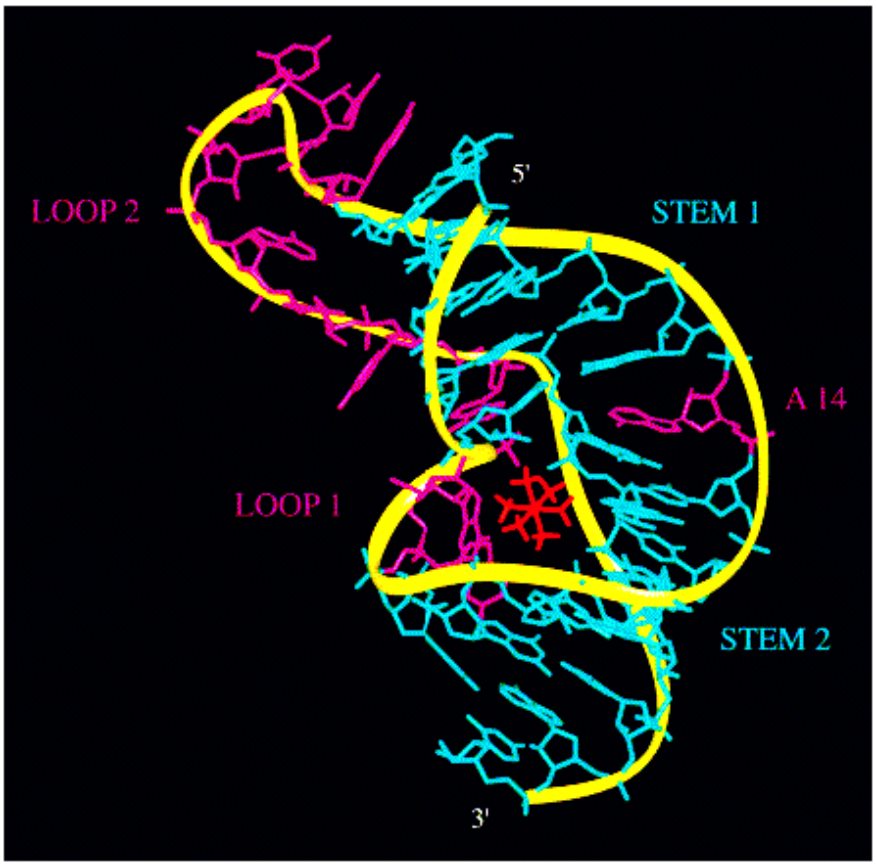

Figure 7. Lowest energy structure of the VPK pseudoknot with $Co(NH_3)_6^{3+}$ shown in the binding pocket. Loops and the junction A14 nucleotide are shown in magenta, stems in cyan, and the $Co(NH_3)_6^{3+}$ ion is shown in red. $Co(NH_3)_6^{3+}$ binds in a binding pocket formed by nucleotides in loop 1 and the major groove of stem 2.

lation protocol produced a family of structures having different positions and orientations of the $Co(NH_3)_6^{3+}$. Each of the 26 final structures was analyzed for hydrogen-bonding interactions (Figure 8). Hydrogen bonds were defined as bond lengths between the proton on the donor atom and the acceptor atom shorter than 2.5 Å with a bond angle of 180(±60)°. Hydrogen bonds were found from the $Co(NH_3)_6^{3+}$ protons to the *pro*-Sp oxygen atom of A6, G7, U8, G9, G10, G29, the *pro*-Rp oxygen atom of C5, A6, G7, U8, and the 2′ hydroxyl of C5, A6, G7, G28. Hydrogen bonds from $Co(NH_3)_6^{3+}$ protons to the bases were observed to the N7 of A6, G7, G9, G10, G11, G28 and G29 and the O6 of G7, G10, G11, G28 and G29, as well as the N3 of A6 and G7. All of these hydrogen bond acceptors line the pocket formed by the sharp turn of loop 1 into stem 2, and are the major determinants of the stabilization of this turn by the metal ion. The rapid tumbling of $Co(NH_3)_6^{3+}$ within the binding pocket allows it to interact with any of these hydrogen bond acceptors.

Comparison with other metal ion binding sites

General trends that have been recently observed in divalent metal ion binding to RNA are also observed in the VPK pseudoknot. The $Co(NH_3)_6^{3+}$ ion binds in a somewhat distorted major groove and interacts with non-bridging phosphate oxygen atoms and purine bases, especially the O6 and N7 of guanine residues (Correl *et al.*, 1997; Cate & Doudna, 1996; Pan *et al.*, 1993; Scott *et al.*, 1995; Pley *et al.*, 1994). The divalent ion binding site reported here, however, is substantially different from the site that has been identified in tandem G·U base-pairs in the P5b (Cate & Doudna, 1996; Kieft & Tinoco, 1997), P5 (Cate & Doudna, 1996; Colmenarejo & Tinoco, 1999), and P1 (Allain & Varani, 1995) helices of the *T. thermophila* group I intron. In this type of site the divalent ion binds in the major groove to tandem G·U base-pairs by hydrogen bonding to the O6 and N7 of the guanine bases. The uracil carbonyl group increases the electronegativity of the surface of the major groove and provides a concave surface for metal ion binding. The ion does not interact with the ribose phosphate backbone. Substituting the G·U pairs with G·C base-pairs diminishes binding to $Co(NH_3)_6^{3+}$, presumably due to the disruption of the electronegative surface and greater steric hindrance upon the replacement of the U carbonyl with the C amino group (Kieft & Tinoco, 1997).

The binding of $Co(NH_3)_6^{3+}$ to the VPK pseudoknot more closely resembles the binding site seen in the P5c region of the group I intron (Cate & Doudna, 1996) and the binding sites of the five metal ions seen in the recently solved crystal structure of a 5 S rRNA domain (Correll *et al.*, 1997). In these binding sites the metal ion complex simultaneously interacts with non-bridging phosphate oxygen atoms and base functional groups. Both direct coordination and outer sphere coordination of the metal ion are observed in these binding

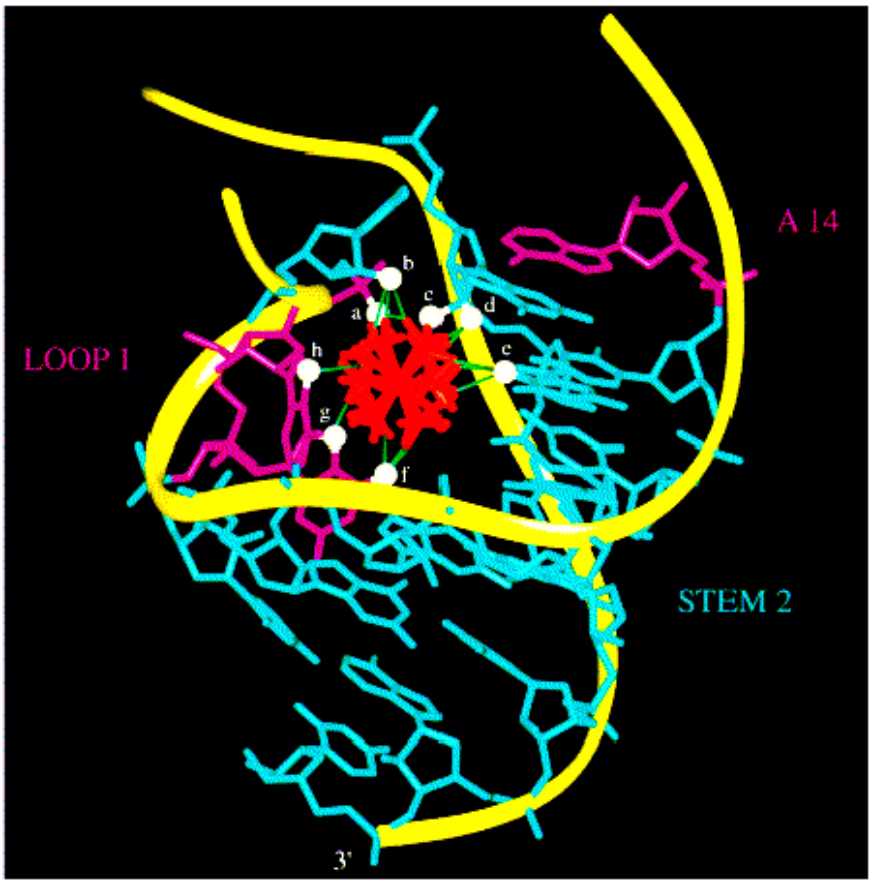

Figure 8. Close up view of the binding pocket for the lowest energy structure showing energetically equivalent orientations of the $Co(NH_3)_6^{3+}$ ion and the hydrogen-bonding pattern observed. Loop 1 and the junction A14 nucleotide are shown in magenta, stem 2 in cyan, $Co(NH_3)_6^{3+}$ in red, hydrogen bond acceptor atoms are shown as white balls, and hydrogen bonds are green. Hydrogen bonds are seen from $Co(NH_3)_6^{3+}$ to the (a) A6 *pro*-Rp oxygen atom, (b) C5 2′ hydroxyl group, (c) G29 *pro*-Sp oxygen atom, (d) G28 2′ hydroxyl group, (e) G29 N7, (f) G7 O6, (g) G7 N7, and (h) A6 N7. Similar analysis for other members of the structural family, reveals slightly different hydrogen-bonding patterns.

sites. The metal in $Co(NH_3)_6^{3+}$ cannot directly coordinate to RNA groups, and therefore serves as a probe of sites that do not involve direct coordination. In the case of the $Co(NH_3)_6^{3+}$ binding to the VPK pseudoknot, the placement of loop 1 in the major groove of stem 2, as well as the perturbation of stem 2 to accommodate this short loop, creates a unique pocket where the interactions between $Co(NH_3)_6^{3+}$ and the loop 1 phosphate, 2′ hydroxyl, and base functional groups makes up for the generally unfavorable binding to the G·C base-pairs in the major groove. The substitution of G·U for G·C base-pairs in stem 2 should create a higher affinity binding site.

Comparison with metal binding predictions

Calculation of the electrostatic surface of the VPK pseudoknot reveals the pocket formed by loop 1 and stem 2 to be among the most electrostatically negative regions of the pseudoknot. Hermann & Westhoff (1998), have demonstrated the use of Brownian dynamics simulations to predict metal-ion binding sites within RNA folds determined by NMR, including the VPK pseudoknot. This approach simulates the trajectories of positively charged spheres subject to the effect of both random Brownian movement and the electrostatic field of the RNA molecule in order to identify metal-ion binding pockets. The application of this simulation to the VPK pseudoknot predicted three metal-ion binding sites (Hermann & Westhoff, 1998). The first metal ion is predicted to bind to G4 and C5 in stem 1 and A25 and A26 in loop 2, the second is predicted to bind to A6 and G7 in loop 1, and the third to G7 in loop 1 and G9 and G10 in stem 2. The last two predicted sites probably correspond to the single $Co(NH_3)_6^{3+}$ site identified by NMR. The $Co(NH_3)_6^{3+}$ binding site can in fact contact all the residues in these two predicted sites simultaneously. There is no NMR evidence that a $Co(NH_3)_6^{3+}$ binding site exists at the predicted binding site of G4 and C5 in stem 1 and A25 and A26 in loop 2. It is important to note that the Brownian dynamics simulation was applied to the previously published VPK structure (Shen &

Tinoco, 1995). We find that the position of loop residues vary considerably within the family of structures compatible with the NMR data. Repeating the simulation with other low energy members of the structural family would show whether predicted metal-ion sites involving loops are influenced by the choice of structure within a family.

Metal ions in frameshifting pseudoknots

Numerous mutational studies have been done to deduce the structural properties of frameshifting pseudoknots that are important for function (Chamorro *et al*., 1992; Brierley *et al*., 1991; Brierley, 1995; ten Dam *et al*., 1994). Three solution NMR structures (Shen & Tinoco, 1995; Kang & Tinoco, 1997; Du *et al*., 1997) and one X-ray crystal structure (Su *et al*., 1999) of frameshifting pseudoknots, as well as an NMR structure of one non-frameshifting mutant (Kang *et al*., 1996) have been obtained in an attempt to deduce a frameshifting mechanism. It has been difficult to identify conserved structural features among different frameshifting sequences that provide insight into the frameshifting mechanism. Precise maintenance of frameshift levels (Dinman & Wickner, 1992), as well as variation in frameshifting levels among different viruses, suggests that viruses may use modification of the pseudoknot frameshifting signal to fine tune the level of frameshifting required by each virus (ten Dam *et al*., 1995). If this is true, then the general requirement of a pseudoknot as a frameshift signal may be conserved, while special features in each pseudoknot regulate the level of frameshifting. Nevertheless, several structural features are conserved. One of the highly conserved structural features of pseudoknots involved in high efficiency retroviral −1 frameshifting is a very short loop 1 crossing the major groove of stem 2. The length of loop 1 is generally one or two residues and stem 2 is generally five to seven base-pairs (Brierley, 1995). A sharp turn at the junction of loop 1 and stem 2 is therefore required with close packing between loop 1 residues and the major groove of stem 2. This turn can be stabilized by an RNA-RNA interaction such as a loop residue to stem residue hydrogen bond, or through the involvement of a metal ion, both of which may be direct or water mediated. In the case of the VPK pseudoknot this turn is stabilized by a divalent metal ion.

The only other frameshifter pseudoknot structure that demonstrates detailed interactions of metal ions is the X-ray crystal structure of the pseudoknot from beet western yellow virus (BWYV; Su *et al*., 1999). In the BWYV pseudoknot, this sharp turn from loop 1 into stem 2 is mediated by a hydrogen bond between a loop phosphate oxygen atom (corresponding to the A6 non-bridging phosphate oxygen atom in VPK) and the N4 of a cytosine in the 3′ closing base-pair of stem 2 (corresponding to the U8 in VPK). The turn is stabilized by an organized network of water molecules which hydrogen bond to non-bridging phosphate oxygen atoms throughout the turn. It is not clear that stabilization of this turn in BWYV is a general feature of frameshifter pseudoknots, since the sequence of loop 1 can vary from one virus to another and the identity of the first base-pair of stem 2 also varies. Also, the structure of the BWYV pseudoknot does not reveal the role of Mg^{2+} in stabilization of the pseudoknot structure, since Mg^{2+} is observed to bind at the 5′-terminal triphosphate group, where it does not mediate any pseudoknot-specific interactions. Su and co-workers rationalize that the large concentration of Na^+ (relative to Mg^{2+}) present in their crystallization buffer leads to stabilization of the pseudoknot structure by Na^+, rather than Mg^{2+}. In the BWYV pseudoknot, a Na^+ is seen to bind in the minor groove of stem 1, interacting with bases in stem 1 and loop 2. It is rather unlikely that this Na^+ ion is exactly mimicking the role of a divalent ion considering that the Na^+ has a tetrahedral coordination geometry while the Mg^{2+} coordination geometry is octahedral. Furthermore, divalent metal ions have not been shown to generally bind in the minor groove of RNA and in this case would probably interfere with the minor groove triplex that is formed between loop 2 and stem 1 (Su *et al*., 1999).

The stabilization of the loop 1 to stem 2 turn and of the close proximity of loop 1 and stem 2 by a divalent metal ion may be a more general feature of this type of frameshifter pseudoknot regardless of sequence, as is evident from the extensive non-sequence-specific interactions to the phosphate oxygen atoms and 2′-hydroxyl groups of the backbone throughout the turn. Interactions with the base functional groups in stem 2, particularly the O6 and N7 of guanine bases will, for the most part, be conserved due to high G·C content of stem 2 in frameshifting pseudoknots. In fact, G·U base-pairs may form a higher affinity binding site by replacing the C amino group with a U carbonyl group. Furthermore substitution of G·C base-pairs with A·U base-pairs will provide a major groove surface very similar to the surface formed by G·C base-pairs. In this case the G carbonyl group has been replaced by the A amino, but the C amino has been replaced by the U carbonyl group.

Conclusion

Using $Co(NH_3)_6^{3+}$ as a probe for Mg^{2+}, this study describes the detailed interaction of a divalent metal ion with an RNA pseudoknot in solution. The structure is generally well defined, although internal dynamics in loop 2 do not allow the precise positioning of loop 2 relative to the other regions of the pseudoknot. The metal ion binding pocket formed by loop 1 residues and the major groove of stem 2 provides a surface lined with phosphate oxygen atoms, 2′ hydroxyl groups, and hydrogen bond acceptors in the bases. Binding of the metal ion stabilizes the sharp turn of loop 1

into stem 2 and the close proximity between loop 1 and the major groove of stem 2. Although the binding is weak ($K_d = 5(\pm 3)$ mM), binding of Mg^{2+} to VPK is likely to be biologically significant due to the high intracellular concentration of Mg^{2+} (30 mM) (Cowan, 1995) and the absence of significant concentrations of other multivalent ions (Feig & Uhlenbeck, 1999). A one to two nucleotide loop 1, five to seven base-pair stem 2, and the availability of numerous non-sequence-specific hydrogen bond acceptors, all conserved features of this type of frameshifter pseudoknot, define the site of Mg^{2+} in stabilization of the pseudoknot and suggests that this is a general feature of this type of frameshifter pseudoknot. It is becoming increasingly clear that in order to understand RNA folding, we will have to learn the ''rules'' by which metal ions bind to RNA and facilitate the formation of compact and complex three-dimensional structures that are essential for function. In the VPK pseudoknot, a divalent metal ion brings together a single-stranded region of the RNA molecule with a helical region, and stabilizes a sharp turn in the molecule. Electrostatic attraction to the phosphates plus water-mediated hydrogen bonds to acceptors on the backbone and the bases provide the binding energy. Because pseudoknots, sharp turns, and close packing of helices and single-stranded regions are general features of RNA structures, we expect that metal ion stabilization of this type of tertiary interaction will be a common feature of RNA folds.

Materials and Methods

Sample preparation

RNA oligonucleotides were transcribed *in vitro* using phage T7 RNA polymerase and synthetic DNA templates (Milligan *et al.*, 1987; Wyatt *et al.*, 1991). RNA from transcription reactions was purified by denaturing 20% (w/v) polyacrylamide gel electrophoresis, removed from gel slices by electro-elution (Simon & Schuster), and concentrated by ethanol precipitation. RNA pellets were dissolved in a 5 mM EDTA solution and then dialyzed in two steps. The first step consisted of dialysis at 4°C against 5 mM EDTA to chelate any divalent cations. In the second step, RNA samples were extensively dialyzed at 4°C against a buffer solution consisting of 10 mM sodium phosphate, 200 mM NaCl, 100 μM EDTA (pH 6.4). Cobalt (III) hexammine chloride was purchased from Sigma. Stock solution concentrations of cobalt (III) hexammine were determined by mass and verified by absorbance at 470 nm ($\varepsilon = 56(\pm 1)\ M^{-1}cm^{-1}$) (Kieft, 1997).

Selective ^{13}C-labeling of RNA

Selectively ^{13}C-labeled nucleoside triphosphates were chemically synthesized and enzymatically phosphorylated as described (SantaLucia *et al.*, 1995). RNA oligonucleotides selectively ^{13}C-labeled at adenine C8 and uracil C6 were *in vitro* transcribed using $^{13}C8$-labeled ATP and $^{13}C6$-labeled UTP and unlabeled GTP and CTP as described (Shen & Tinoco, 1995). Selectively labeled RNA oligonucleotides were purified and dialyzed as described above.

UV absorbance melting curves

UV absorbance melting curves were recorded on a Gilford 250 spectrophotometer connected to a PC. Heating was controled by a Gilford 2527 Thermo-programmer also connected to the PC. RNA sample concentrations for melting experiments were 4 μM. Samples were heated to 70°C for 30 seconds and then cooled to 0°C for two minutes prior to data acquisition. Four samples were heated simultaneously at a heating rate of 0.5 deg. C per minute. The data were subsequently processed using Kaleidagraph software. Data were smoothed over a 5 deg. C window and absorbance was plotted against temperature. Melting temperatures were determined from the maximum values of the derivative of absorbance with respect to temperature. Standard enthalpy changes were estimated from the full widths at half height of the derivative curves.

Equilibrium dialysis

The large amount of RNA needed for equilibrium dialysis experiments prevented us from studying the pseudoknot. Instead we used the P5b hairpin RNA studied by Kieft & Tinoco (1997) as a model molecule. P5b RNA in 10 mM sodium phosphate, 200 mM Na^+, 100 μM EDTA (pH 6.4) was placed into one half-cell, and $Co(NH_3)_6^{3+}$ in the same buffer was placed into the other half-cell. Equilibrium dialysis experiments were performed in 150 μl half-cells separated by a 2000 molecular mass cut off dialysis membrane. The samples were allowed to equilibrate at 4°C for 24 hours. This equilibration temperature and time were determined by monitoring $Co(NH_3)_6^{3+}$ concentration as it diffused across the membrane in the absence of any RNA. Free $Co(NH_3)_6^{3+}$ concentrations were determined using inductively coupled plasma (ICP) spectroscopy to measure the concentration of cobalt in the half-cell without RNA. Bound $Co(NH_3)_6^{3+}$ concentration was determined using ICP spectroscopy to determine the concentration of cobalt in the half-cell containing RNA and subtracting the free cobalt concentration. Equilibrium dissociation binding constants were determined by Scatchard analysis of the data.

NMR spectroscopy

Sample concentrations for NMR experiments, determined by UV absorbance at 260 nm, were approximately 2 mM with the exception of one dimensional (1D) titration experiments where the RNA concentrations were typically 400 μM. Samples containing Mg^{2+} were prepared by directly adding 1 M $MgCl_2$ to the dialyzed sample to a final Mg^{2+} concentration of 5 mM. This Mg^{2+} concentration has been previously determined to be sufficient for pseudoknot stabilization (Shen & Tinoco, 1995). Samples containing $Co(NH_3)_6^{3+}$ were prepared by directly adding 0.5 M $Co(NH_3)_6^{3+}$ to the dialyzed sample to a final $Co(NH_3)_6^{3+}$ concentration which was equimolar to the RNA concentration. Samples were titrated with 1 M $MgCl_2$ or 0.5 M $Co(NH_3)_6^{3+}$ to achieve the desired concentrations. Samples for exchangeable proton experiments were lyophilized to dryness and redissolved in 90% H_2O/10% ^2H_2O. Samples used for non-exchangeable proton experiments were lyophilized to dryness, lyophilized twice from 99.96% ^2H_2O, and

then dissolved in 99.96 % ^2H_2O. Trace amounts of TSP (3-(trimethylsilyl)propionate-*d*4) were added to all samples as a chemical shift reference standard. All NMR spectra were processed using FELIX 95.0 (Biosym Technologies, Inc.).

Exchangeable proton 1D spectra were recorded on a GE GN-500 spectrometer equipped with a Bruker HX probe. Solvent suppression was achieved by the jump-return method with the excitation maximum set between the imino and amino/aromatic resonances (Plateau & Guéron, 1982). A spectral width of 10,000 Hz was used to collect 4096 complex data points with a relaxation delay of two seconds.

Two-dimensional spectra were collected on a Bruker AMX-600 spectrometer equipped with a Bruker triple resonance triple-axis gradient probe or a Bruker DRX-500 spectrometer equipped with a Nalorac triple resonance *z*-axis gradient probe. Unless otherwise stated, 400-512 blocks of 32-80 scans consisting of 2048-4096 complex points were collected over a spectral width of 10,000 Hz (DRX-500) in H_2O, or over spectral widths of 4000 Hz (DRX-500) or 5000 Hz (AMX-600) in ^2H_2O. The relaxation delay was set to two seconds for all experiments.

NOESY experiments in H_2O were recorded at 150 ms, 300 ms, and 400 ms mixing times at temperatures of 15 and 30 °C in Mg^{2+} and 20 °C and 35 °C in $Co(NH_3)_6^{3+}$. Solvent suppression was accomplished by replacing the last pulse in the NOESY sequence with a jump-return sequence and applying a *z*-gradient pulse during the mixing time. NOESY experiments in ^2H_2O were recorded using a presaturation pulse for suppression of the residual HDO peak. Zero and double quantum artifacts at short mixing times were suppressed by applying a *z*-gradient pulse during the mixing time and incrementing the mixing time from one block to the next for a total of 5 ms incrementation over the full experiment time. The ^2H_2O NOESY spectra was acquired at 60 ms, 150 ms, 300 ms, and 400 ms mixing times at temperatures of 15 and 30 °C for Mg^{2+} and 20 °C and 35 °C for $Co(NH_3)_6^{3+}$. DQF-COSY experiments were recorded using a presaturation pulse for suppression of the residual HDO peak. The ^{13}C-resolved HSQC-NOESY experiment was done in 90 % H_2O/10 % ^2H_2O. The pulse sequence of Majumdar & Zuiderweg (1993) was used to provide water suppression *via* pulsed field gradients without introducing an unfavorable excitation profile.

Structural constraints

Distance constraints were used to maintain hydrogen bonds for base-pairs which clearly formed as seen in the H_2O NOESY experiments. Four distance constraints were used for the G·C base-pairs, three for the A·U base-pairs, and five for the G·U base-pairs. The hydrogen bond range was set to ±0.1 Å. All observed imino to imino NOE crosspeaks were from G iminos in G·C base-pairs, and were assigned a distance range of 3.2 to 4.5 Å. Intra- and intermolecular NOE crosspeaks for non-exchangeable protons were classified into distance range categories based on their intensities in 60 ms, 150 ms, and 300 ms mixing time NOESY experiments in ^2H_2O. $Co(NH_3)_6^{3+}$ protons were treated as non-exchangeable, since they do not exchange on the time-scale of one block of scans (Anderson *et al.*, 1943). NOE crosspeaks to the $Co(NH_3)_6^{3+}$ were referenced to a pseudo-atom at the position of the cobalt atom, with appropriate distance corrections. NOE crosspeaks were classified as strong (1.8-3.2 Å), medium (2.0-4.0 Å), weak (2.5-5.0 Å), and very weak (3.0-6.0 Å). Crosspeaks which could arise from a spin diffusion pathway were put into a distance range of 2.0-5.0 Å.

Ribose sugar conformations, or δ torsion angles, were determined based on H1′-H2′ scalar couplings observed in DQF-COSY experiments. Backbone torsion angles (α, β, γ, ε, and ζ) were constrained to standard *A*-form (Saenger, 1984) in the helical stems of the pseudoknot based on observed scalar couplings and NOE connectivities that indicated *A*-form structure. The backbone torsion angles of the opening and closing base-pairs of stem 2, closing base-pair of stem 1, and all loop nucleotides were not constrained.

Structure calculations

The molecular dynamics program X-PLOR was used to do the structure calculations (Brünger, 1993). The $Co(NH_3)_6^{3+}$ complex ion was built using the Builder module within the INSIGHT II suite of programs (Biosym Technologies, Inc.). Partial charges and Lennard-Jones potentials for the $Co(NH_3)_6^{3+}$ ion were taken from the ESFF forcefield values. The structure of the $Co(NH_3)_6^{3+}$ ion prepared in this manner is in good agreement with the published crystal structure (Kruger & Reynhardt, 1978). A total of 100 starting structures were generated with randomized backbone torsion angles α, β, γ, δ, ε, and ζ, and randomized positioning of the $Co(NH_3)_6^{3+}$ complex ion. The structure calculation was performed in three stages. The global fold protocol consisted of terms including bond lengths, bond angles, improper angles, and the NMR-derived distance and torsion angle constraints. The bond angle and bond length force constants were set to 1000 kcal mol^{-1} $Å^{-2}$ and 500 kcal mol^{-1} rad^{-2}, respectively. The NOE force constant was set to 50 kcal mol^{-1} $Å^{-2}$ and the torsion angle force constant was initially set to 5 kcal mol^{-1} rad^{-2} and increased throughout the calculation to a final value of 50 kcal mol^{-1} rad^{-2}. The protocol consisted of 500 cycles of energy minimization of the randomized starting structure. This was followed by restrained molecular dynamics (rMD) at 1000 K followed by rMD during cooling to 300 K. Finally 100 cycles of energy minimization were done. All NOE distance constraints were used during the global fold protocol, however intermolecular $Co(NH_3)_6^{3+}$ to the RNA distance constraints were given a loose, initial range of 0-10 Å. Only torsion angles specifying the sugar puckers and keeping amino groups in the plane of the base-pairs were used during the global fold protocol. The second stage of structure calculation was a refinement of the converged structures. All of the previous terms used in the global fold were used for the structure refinement with the addition of the backbone torsion angles. The intermolecular $Co(NH_3)_6^{3+}$ to RNA distance constraints were now assigned semi-quantitative values according to the NOE data using the same criteria and categories as for the RNA non-exchangeable protons. The refinement protocol consisted of 500 cycles of energy minimization, rMD at 1000 K during which the backbone torsion angles were introduced in two stages: first, β,γ, and ε were introduced, followed by α and ζ, rMD while cooling to 300 K, and 100 cycles of energy minimization. In the final stage of structure calculation, these refined structures underwent rMD at 300 K followed by 3000 cycles of energy minimization which now included all the terms used in the structure refinement with the addition of Lennard-Jones

potentials. This structure calculation protocol resulted in a family of converged structures which were viewed using INSIGHT II.

Acknowledgments

This research was supported in part by National Institute of Health Grant GM 10840, by the Department of Energy Grant DE-FG03-86ER60406, and through instrumentation grants from the Department of Energy (DE-FG05-86ER75281) and from the National Science Foundation (DMB 86-09305). We thank Ms Barbara Dengler for managing the laboratory, Mr David Koh for synthesizing DNA oligonuceotides, and Dr Jeffrey Pelton for valuable NMR advice.

References

Allain, F. H. T. & Varani, G. (1995). Divalent metal ion binding to a conserved wobble pair defining the upstream site of cleavage of group I self-splicing introns. *Nucl. Acids Res.* **23**, 341-350.

Anderson, C. F. & Record, M. T., Jr (1995). Salt-nucleic acid interactions. *Annu. Rev. Phys. Chem.* **46**, 657-700.

Anderson, J. S., Briscoe, H. V. A. & Spoor, N. L. (1943). Interchange of hydrogen isotopes with complex salts. Part I. Kinetics of the interchange with the luteocobaltic complex. *J. Chem. Soc.*, 361-367.

Brierley, I. (1995). Ribosomal frameshifting on viral RNAs. *J. Gen. Virol.* **76**, 1185-1892.

Brierly, I., Rolley, N. J., Jenner, A. J. & Inglis, S. C. (1991). Mutational analysis of the RNA pseudoknot component of a coronavirus ribosomal frameshifting signal. *J. Mol. Biol.* **220**, 889-902.

Brünger, A. T. (1993). *X-PLOR: A System for Crystallography and NMR, Version 3.1*, Yale University, New Haven, USA, CT.

Cate, J. H. & Doudna, J. A. (1996). Metal-binding sites in the major groove of a large ribozyme domain. *Structure,* **4**, 1221-1229.

Cate, J. H., Gooding, A. R., Podell, E., Zhou, K., Golden, B. L., Kundrot, C. E., Cech, T. R. & Doudna, J. A. (1996). Crystal structure of a group I intron ribozyme domain: principles of RNA packing. *Science,* **273**, 1678-1685.

Chamorro, M., Parkin, N. & Varmus, H. E. (1992). An RNA pseudoknot and an optimal heptameric shift site are required for highly efficient ribosomal frameshifting on a retroviral messenger RNA. *Proc. Natl Acad. Sci. USA,* **89**, 713-717.

Chen, X., Chamorro, M., Lee, S. I., Shen, L. X., Hines, J. V., Tinoco, I., Jr & Varmus, H. E. (1995). Structural and functional studies of retroviral RNA pseudoknots involved in ribosomal frameshifting: nucleotides at the junction of the two stems are important for efficient ribosomal frameshifting. *EMBO J.* **14**, 842-852.

Colmenarejo, G. & Tinoco, I., Jr (1999). Structure and thermodynamics of metal binding in the P5 helix of a group I intron ribozyme. *J. Mol. Biol.* In the press.

Correl, C. C., Freeborn, B., Moore, P. B. & Steitz, T. A. (1997). Metals, motifs, and recognition in the crystal structure of a 5 S rRNA domain. *Cell,* **91**, 705-712.

Cowan, J. A. (1993). Metallobiochemistry of RNA. Co $(NH_3)_6^{3+}$ as a probe for Mg^{2+}(aq) binding sites. *J. Inorg. Biochem.* **49**, 171-175.

Cowan, J. A. (1995). *The Biological Chemistry of Magnesium*, VCH, New York.

Dinman, J. D. & Wickner, R. B. (1992). Ribosomal frameshifting efficiency and *gag/gag-pol* ratio are critical for yeast M1 double-stranded RNA virus propagation. *J. of Virol.* **66**, 3669-3676.

Doudna, J. A. & Doherty, E. A. (1997). Emerging themes in RNA folding. *Folding Des.* **2**, R65-R70.

Draper, D. E. (1985). On the coordination properties of Eu^{3+} bound to tRNA. *Biophys. Chem.* **21**, 91-101.

Du, Z. H., Holland, J. A., Hansen, M. R., Giedroc, D. P. & Hoffman, D. W. (1997). Base-pairings within the RNA pseudoknot associated with the simian retrovirus-1 gag-pro frameshift site. *J. Mol. Biol.* **270**, 464-470.

Feig, A. L. & Uhlenbeck, O. C. (1999). The role of metal ions in RNA biochemistry. In *The RNA World* (Gesteland, R. F., Cech, T. R. & Atkins, J. F., eds), 2nd edit., pp. 287-318, Cold Spring Harbor Laboratory Press, Plainview, USA, NY.

Ferré-D'Amaré, A. R., Zhou, K. H. & Doudna, J. A. (1998). Crystal structure of a hepatitis delta virus ribozyme. *Nature,* **395**, 567-574.

Guerrier-Takada, C., van Belkum, A., Pleij, C. W. A. & Altman, S. (1988). Novel reactions of RNase P with a t-RNA like structure in turnip yellow mosaic virus RNA. *Cell,* **53**, 267-272.

Haenni, A.-L., Joshi, S. & Chapeville, F. (1982). tRNA-like structures in the genomes of RNA viruses. *Prog. Nucl. Acid Res. Mol. Biol.* **27**, 85-104.

Hermann, T. & Westhof, E. (1998). Exploration of metal ion binding sites in RNA folds by Brownian dynamics simulations. *Structure,* **6**, 1303-1314.

Holbrook, S. R., Sussman, J. L., Warrant, R. W., Church, G. M. & Kim, S. H. (1977). RNA-ligand interactions: (I) magnesium binding sites in yeast tRNAPhe. *Nucl. Acids Res.* **8**, 2811-2820.

Jack, A., Ladner, J. E., Rhodes, D., Brown, R. S. & Klug, A. (1977). A crystallographic study of metal-binding to yeast phenylalanine transfer RNA. *J. Mol. Biol.* **111**, 315-328.

James, B. D., Olsen, G. J., Liu, J. & Pace, N. R. (1988). The secondary structure of ribonuclease P RNA, the catalytic element of a ribonucleoprotien enzyme. *Cell,* **52**, 19-26.

Joshi, R. L., Joshi, S., Chapeville, F. & Haenni, A. L. (1983). t-RNA like structures of plant viral RNAs: comformational requirements for adenylation and aminoacylation. *EMBO J.* **2**, 1123-1127.

Jou, R. W. & Cowan, J. A. (1991). Ribonuclease-H activation by inert transition-metal complexes. Mechanistic probes for metallocofactors: insights on the metallobiochemistry of divalent magnesium ion. *J. Am. Chem. Soc.* **113**, 6685-6686.

Kalurachchi, K. & Nikonowicz, E. P. (1998). NMR structure determination of the binding site for ribosomal protein S8 from *Escherichia coli* 16 S rRNA. *J. Mol. Biol.* **280**, 639-654.

Kang, H. & Tinoco, I., Jr (1997). A mutant pseudoknot that promotes ribosomal frameshifting in mouse mammary tumor virus. *Nucl. Acids Res.* **25**, 1943-1949.

Kang, H., Hines, J. V. & Tinoco, I., Jr (1996). Conformation of a non-frameshifting RNA pseudoknot from mouse mammary tumor virus. *J. Mol. Biol.* **259**, 135-147.

Kieft, J. S. (1997). Structure and thermodynamics of a metal ion binding site in the RNA major groove: cobalt (III) hexammine as a probe, PhD thesis, University of California, Berkeley.

Kieft, J. S. & Tinoco, I., Jr (1997). Solution structure of a metal-binding site in the major groove of RNA complexed with cobalt(III)hexammine. *Structure,* **5**, 713-721.

Kolk, M. H., van der Graaf, M., Wijimenga, S. S., Pleij, C. W., Heus, H. A. & Hilbers, C. W. (1998). NMR structure of a classical pseudoknot: interplay of single- and double-stranded RNA. *Science,* **280**, 434-438.

Kruger, G. J. & Reynhardt, E. C. (1978). Hexammineco-balt (III) chloride. *Acta Crystallog. sect. B,* **34**, 915-917.

Laggerbauer, B., Murphy, F. L. & Cech, T. R. (1984). Two major tertiary folding transitions of the *Tetrahymena* catalytic RNA. *EMBO J.* **13**, 2669-2676.

Majumdar, A. & Zuiderweg, E. R. P. (1993). Improved ^{13}C-resolved HSQC-NOESY spectra in H_2O using pulsed field gradients. *J. Magn. Reson. series B,* **102**, 242-244.

Milligan, J. F., Groebe, D. R., Witherell, G. W. & Uhlenbeck, O. C. (1987). Oligoribonucleotide synthesis using T7 RNA polymerase and synthetic DNA templates. *Nucl. Acids Res.* **15**, 8783-8798.

Moazed, D. & Noller, H. F. (1987). Interaction of antibiotics with functional sites in 16 S ribosomal RNA. *Nature,* **327**, 389-394.

Nixon, P. L. & Giedroc, D. P. (1998). Equilibrium unfolding (folding) pathway of a model H-type pseudoknotted RNA: the role of magnesium ions in stability. *Biochemistry,* **37**, 16116-16129.

Pan, T., Long, D. M. & Uhlenbeck, O. C. (1993). Divalent metal ions in RNA folding and catalysis. In *The RNA World* (Gesteland, R. F. & Atkins, J. F., eds), pp. 271-302, Cold Spring Harbor Laboratory Press, Plainview, NY).

Plateau, P. & Guéron, M. (1982). Exchangeable proton NMR without base-line distortion, using new strong-pulse sequences. *J. Am. Chem. Soc.* **104**, 7310-7311.

Pleij, C. W. A., Rietveld, K. & Bosch, L. (1985). A new principle of RNA folding based on pseudoknotting. *Nucl. Acids Res.* **13**, 1717-1731.

Pley, H. W., Flaherty, K. M. & McKay, D. B. (1994). Three-dimensional structure of a hammerhead ribozyme. *Nature,* **372**, 68-74.

Qui, H., Kahuarachchi, K., Du, Z., Hoffman, D. W. & Giedroc, D. P. (1996). Thermodynamics of folding fo the RNA pseudoknot of the T4 gene 32 autoregulatory messenger RNA. *Biochemistry,* **35**, 4176-4186.

Rietveld, K., van Poelgeest, R., Pleij, C. W. A., van Boom, J. H. & Bosch, L. (1982). The t-RNA like structure at the 3′ terminus of turnip yellow mosaic virus RNA. Differences and similarities with canonical tRNA. *Nucl. Acids Res.* **10**, 1929-1946.

Roberts, G. C. K. (1993). *Editor of NMR of Macromolecules: A Practical Approach*, IRL Press, Cambridge.

Robinson, H. & Wang, A. H.-J. (1996). Neomycin, spermine, and hexamminecobalt (III) share common structural motiffs in converting *B*- to *A*-DNA. *Nucl. Acids Res.* **24**, 676-682.

Saenger, W. (1984). *Principles of Nucleic Acid Structure* (Cantor, C. R., ed.), Springer-Verlag, New York.

SantaLucia, J., Shen, L. X., Cai, Z. P., Lewis, H. & Tinoco, I., Jr (1995). Synthesis and NMR of RNA with selective isotope enrichment in the bases. *Nucl. Acids Res.* **23**, 4913-4921.

Schimmel, P. (1989). RNA pseudoknots that interact with components of the translation apparatus. *Cell,* **58**, 9-12.

Scott, W. G., Finch, J. T. & Klug, A. (1995). Crystal structure of an all-RNA hammerhead ribozyme: a proposed mechanism for RNA catalytic cleavage. *Cell,* **81**, 991-1002.

Shen, L. X. & Tinoco, I., Jr (1995). The structure of an RNA pseudoknot that causes efficient frameshifting in mouse mammary tumor virus. *J. Mol. Biol.* **247**, 963-978.

Stein, A. & Crothers, D. M. (1976). Conformational changes of transfer RNA. The role of magnesium (II). *Biochemistry,* **15**, 160-167.

Su, L., Chen, L., Egil, M., Berger, J. M. & Rich, A. (1999). A minor groove RNA triplex in the crystal structure of a viral pseudoknot involved in ribosomal frameshifting. *Nature Struct. Biol.* In the press.

Tang, C. K. & Draper, D. E. (1989). Unusual mRNA pseudoknot structure is recognized by a protein translational repressor. *Cell,* **57**, 531-536.

ten Dam, E., Brierly, I., Inglis, S. & Pleij, C. (1994). Identification and analysis of the pseudoknot containing gag-pro ribosomal frameshift signal of simian retrovirus −1. *Nucl. Acids Res.* **22**, 2304-2310.

ten Dam, E. B., Verlaan, P. W. G. & Pleij, C. W. A. (1995). Analysis of the role of the pseudoknot component in the SRV-1 *gag-pro* ribosomal frameshift signal: loop lengths and stability of the stem regions. *RNA,* **1**, 146-154.

Theimer, C. A., Wang, Y., Hoffman, D. W., Krisch, H. M. & Giedroc, D. P. (1998). Non-nearest neighbor effects on the thermodynamics of unfolding of a model mRNA pseudoknot. *J. Mol. Biol.* **279**, 545-564.

Wyatt, J. R., Puglisi, J. D. & Tinoco, I., Jr (1990). RNA pseudoknots-stability and loop size requirements. *J. Mol. Biol.* **214**, 455-470.

Wyatt, J. R., Chastain, M. & Puglisi, J. D. (1991). Synthesis and purification of large amounts of RNA oligonucleotides. *Biotechniques,* **11**, 764-769.

Edited by D. E. Draper

(Received 12 February 1999; received in revised form 3 May 1999; accepted 4 May 1999)

http://www.academicpress.com/jmb

Supplementary material for this paper comprising two Tables is available from JMB Online